Vacuum 209 (2023) 111804

Contents lists available at ScienceDirect

Vacuum

journal homepage: www.elsevier.com/locate/vacuum

A power-free vacuum suitcase for sample transfer and cryogenic optical characterization of sensitive 2D materials

Dongli Wang [1], Di Wu [1], Songjie Feng, Yuang Li, Tai Min, Yi Pan [*]

Center for Spintronics and Quantum Systems, State Key Laboratory for Mechanical Behavior of Materials, Xi'an Jiaotong University, Xi'an, 710049, China

ARTICLE INFO

Keywords:
Vacuum suitcase
Non-evaporable getter
2D materials

ABSTRACT

Although some of the 2D layered materials like graphene and h-BN are stable in ambient condition, many other ones like the magnetic metal halogens CrI_3 might degrade quickly in air due to oxidation or hydrolyzation that drastically affect the intrinsic properties of the pristine samples. Thus, a clean environment is highly demanded for such sensitive 2D materials during storage or transferring between synthesis and characterization setups. Additionally, variable sample temperature is crucial for characterization as well. Here, we demonstrate a specially designed vacuum suitcase that meet these challenges. It utilizes power-free non-evaporable getter pump to provide the ultra-clean vacuum environment for up to 5 samples, which could be maintained at 10^{-8} mbar level for 5 h and 10^{-7} mbar level for more 20 days. One of the samples is stored on a liquid nitrogen cooled (~80 K–300 K) cryogenic stage, which is optimized for optical characterizations (Raman spectroscopy etc.) through a glass window. Such power-free vacuum suitcases would facilitate the clean environment sample transfer and variable temperature optical characterization of as grown sensitive 2D materials.

1. Introduction

In recent years, the two-dimensional (2D) layered materials have attracted lots of research attention since they are considered as promising candidates for the post-Moore era microelectronic, optoelectronic and quantum devices. The natural atomic scale layer thickness and tunable layer interactions of such materials would bring about intriguing physical properties, for example, the 2D ferromagnetism in CrI_3 [1] , $CrBr_3$ [2] , Fe_3GeTe_2 [3] and $Cr_2Ge_2Te_6$ [4]; 2D ferroelectricity in α-In_2Se_3 [5] and 1T′-$MoTe_2$ [6]; charge density wave in TaS_2 [7], $ZrTe_2$ [8] and $TiSe_2$ [9]; Weyl semimetal behavior in 1T′-WTe_2 [10] and 1T′-$MoTe_2$ [11]. These 2D materials are usually obtained by mechanical exfoliation of bulk crystals in glovebox, chemical vapor deposition in tube furnace with inert gas or molecular beam epitaxial (MBE) in ultra-high vacuum (UHV) chambers. In particular, the MBE method could provide samples with pristine surface that is suitable for *in situ* characterization like XPS, LEED, STM and ARPES.

Although some of the 2D materials like graphene and h-BN are known to be stable in air, many others like the magnetic metal halogens CrI_3 and $CrBr_3$ might degrade quickly in ambient condition. The degradation mainly arises from surface physical adsorption and/or chemical reaction with the molecules in air. The physical adsorption would contaminate almost all kinds of 2D materials. It is particularly harmful for the 2D ferroelectric materials since the vertical polarity could be completely compensated by the adsorption layer. The chemical reaction would irreversibly damage the sensitive 2D martials due to oxidation or hydrolyzation [12]. As for the 2D materials based devices, air exposure also gradually spoils the atomically sharp interfaces in the van der Waals heterojunctions. Thus, sample degradation is indeed a crucial problem that hinders the *ex situ* characterization of the intrinsic properties of the 2D materials. Additionally, sample temperature is another critical factor for characterization since many physical properties are temperature dependent and the signal/noise ratio is much better at low temperature. For example, the charge density wave in $CeTe_3$ could be revealed by Raman spectroscopy below 200 K [13]; the twist-angle-dependent exciton in the TMDC heterojunctions can be well elucidated by PL spectroscopy at 80 K [14]. Therefore, it is highly demanding for a specially designed potable sample storage equipment which not only provide long time UHV conditions during transferring between the UHV synthesis and characterization setups, but also facilitate the variable temperature characterization without taking it out of the UHV environment.

* Corresponding author.
E-mail address: yi.pan@xjtu.edu.cn (Y. Pan).
[1] Contributed equally

https://doi.org/10.1016/j.vacuum.2023.111804
Received 20 October 2022; Received in revised form 31 December 2022; Accepted 31 December 2022
Available online 2 January 2023

The UHV suitcase, which is a portable UHV setup, could be an ideal solution if the cryogenic sample stage is added. The early UHV suitcase usually employ a valve regulated lead acid (VRLA) battery powered ion gutter pump to maintain the vacuum condition [15]. For a reasonable UHV maintaining time of a few hours, the VRLA battery need to be at least tens of kilograms. Later, the non-evaporable getter pump (NEG) are incorporated into the ion getter pump, thus the portability could be dogmatically improved [16]. So far, the compact vacuum suitcase with commercial NEG pump or NEG-ion combination pump has been for sample transfer between UHV systems [17–19]. However, the cryogenic sample stage is not available in UHV suitcase so far.

Here we report the design and a prototype model of a power free vacuum suitcase that not only fulfil the requirements of long time sample storage in vacuum, but also could be used for low temperature optical spectroscopic characterization. It is a NEG-only lightweight portable UHV system that is compatible to the flag type MBE sample holder. It could directly connect to other UHV systems via standard metric contact flanges. The high performance UHV condition below 1×10^{-8} mbar could be maintained for 5 h, while the total holding time for pressure below 5×10^{-8} mbar is more than 20 days. More importantly, it could also serve as compact optical cryostat for micro size and big field angle characterization of chemically active MBE samples. This system has been successfully used to transfer $MoTe_2$ thin films synthesized by MBE to another UHV setup for STM characterization.

2. Design of the multifunction vacuum suitcase

Driven by the demanding of transferring MBE sample to a separate system for LT-STM measurement, as well as the routine Raman and PL characterization in a public platform, we have designed a portable vacuum sample transfer, storage and characteristic system. The specific requirements for this system are as follows: 1) Maintaining UHV condition ($<5 \times 10^{-8}$ mbar) for at least a week with power free NEG pump. 2) Receiving and capturing storage flag type sample holder via transfer rod that is compatible to commercial MBE system; 3) Maintaining certain required temperature of the sample mounted on variable temperature stage between 80K and RT; 4) Providing optimized sample to glass window distance for optical spectroscopic characterization. 5) Connecting to other system through a DN40 UHV gate valve flange. Additionally, as UHV setup the whole system should sustain the baked out temperature up to 140 °C, and mounted on a solid and light weighted frame.

2.1. The components and structure of the system

To fulfil the requirement, we design a compact multifunctional vacuum suitcase that combines the functions of conventional vacuum suitcase for sample transfer and UHV cryogenic sample stage for optical measurement, with minimized weight. As shown in Fig. 1(a), the system consists only 9 components (#1–9), which are assembled on a cuboid aluminum alloy frame. The main chamber (#1) is a stainless steel

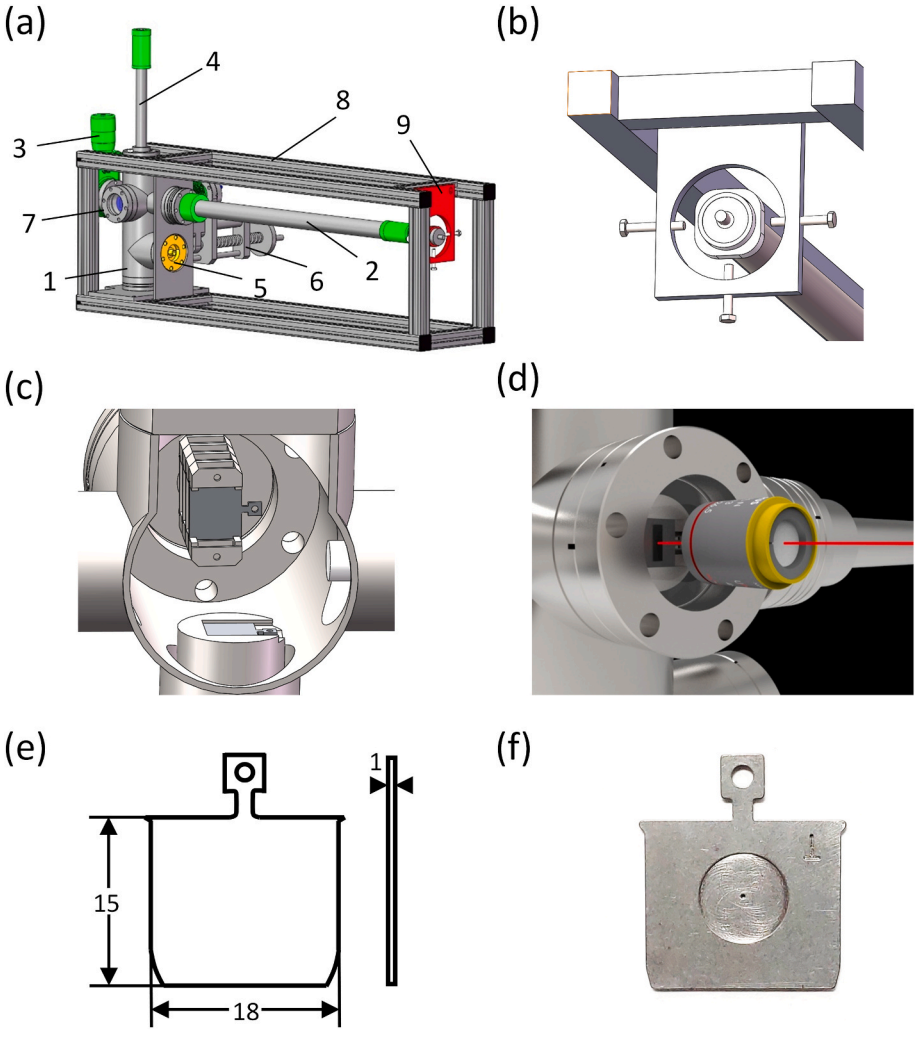

Fig. 1. (a) Over view of the designed vacuum suitcase consisting of (1) a main chamber, (2) a transfer rod, (3) a mini gate valve DN40, (4) a sample storage, (5) a NEG pump, (6) a cryogenic sample stage, (7) a viewport, (8) an aluminum frame, and (9) an adjustment plate. (b) The enlarged view of the fine adjusting mechanism for the transfer rod. (c) Sectional bottom view inside the chamber showing the sample storage, the end of transfer rod and the cryogenic sample stage. (d) The schematic diagram showing the mechanism of the sample under optical characterization. (e) The dimension and (f) the photo of the flag type sample holder. (Unit: mm).

(SS316) cylinder of 2.6 L volume with 6 DN40 ports. The top port of the chamber is connected to a magnetic linear motion (#4) with 5-storey sample storage. There are 4 ports in the upper side wall of the chamber at the same height. The front port is assembled with a mini gate valve (#3) which is for the connection to external UHV chamber during sample exchange. The back port is assembled with a magnetic transfer rod (#2) of 80 cm maximum extending length. The two side ports are assembled with a glass viewport (#7) for optical access and mechanical linear motion (#6) with cryogenic sample stage, respectively. At the lower side wall below the port for the transfer rod, there's another port for the NEG getter pump.

The frame must be very solid, since during sample exchange the metal contact flange connection between UHV systems requires high rigidity and precise alignment. But it also needs to be light weighted as a portable equipment. Therefore, we use the 30 mm width aluminum extrusion profile (6036-T5 aluminum alloy) to construct the frame. It also provides enough protection to the fragile parts and fix the flexible transfer rod. Additionally, using the power free NEG pump instead of battery powered ion getter pump could save a few kilograms of the weight. Benefited from such design, the weight of the whole system is reduced to below 15 kg.

The sample storage and transfer rod are commercial products that match with the flag type sample holder, as shown in Fig. 1(e) and (f). Sample transfer is conducted by linear movement of inserting into and pulling out of the storage slot, which is secured by a rotary mechanism that could lock and unlock the sample holder. Since the smooth sample transfer requires fine tilting adjustment of the transfer rod, we designed a simple crosshair shape tilting adjustment plate, as shown in Fig. 1(b). This plate regulates the X–Y movement at the rare end of the transfer rod. Since the pivot is much closer to the head, rare end movement could easily realize the fine tilt tuning at the head. It has an advantage comparing with the transitional X–Y movement regulation at the head. Additionally, the plate could also provide protection to the transfer rod by firmly fix the end, when the rod is not in use.

2.2. Design of the cryogenic sample stage

In this system, we have integrated a variable temperature cryogenic sample stage for the spectroscopic measurement of the chemically sensitive samples. The sample stage is cooled by directly filling LN_2 into the mini cryostat or pumping cold N_2 evaporated from LN_2 tank. Thus, the temperature could be control by regulating the gas flow rate of external pump. The sample stage is mounted on a linear motion with moving distance of 50 mm in parallel direction towards a glass window. As shown in Fig. 1 (c), when the sample stage is fully retracted, there is enough space in the chamber for the transfer rod to fetch samples from other chambers; when it's approached half way, it could receive sample from the rod; when it's fully approached, it's close enough to the window for the microscopic optical measurement. Since the minimum distance between sample surface and the out surface of the glass window is about 8 mm, micro meter scale spacial resolution could be achieved with suitable objective lens, as demonstrated in Fig. 1(d).

The sample stage is attached to LN_2 cooled mini cryostat designed for microscopy applications, which has similar structure as the commercial Oxford microstatN. The inlet and outlet of the LN_2 container is at the flange, as shown in Fig. 2(a). The position of the sample is indicated by the dashed circle in Fig. 2(b). The container could hold about 125 mL cryogen. Taking LN_2 as an example, the simulation shows the temperature can reach ~80 K with continuous supply of cryogen. The holding time of every refill cycle is 42 min without LN_2 filling. The details of simulation are discussed in section 3.1.

2.3. The NEG-only vacuum maintaining design

The UHV condition of the system is reached by pumping with an external pumping station and baking out at high temperature. During sample transferring period, the vacuum is maintained by using a custom-made NEG pump of Zr-V-Fe alloy (70 wt % Zr, 24.6 wt % V, and 5.4 wt % Fe, produced by Nanjing Huadong Electronics Vacuum Material Co., Ltd.) as the only pump of the system. The structure of the pump is demonstrated in Fig. 3(a) and the photo of the NEG pump used in the vacuum suitcase is shown in Fig. 3(b). The NEG module consists of 20 NEG Zr-V-Fe alloy pills (Φ25 × 2 mm). After fully activation, the pumping speed of NEG pump is ~200, 100, and 45 L/s for H_2, CO, and N_2 gasses, respectively. The NEG pumps produced by the same company has been reported in the literature, which confirmed its good performance.

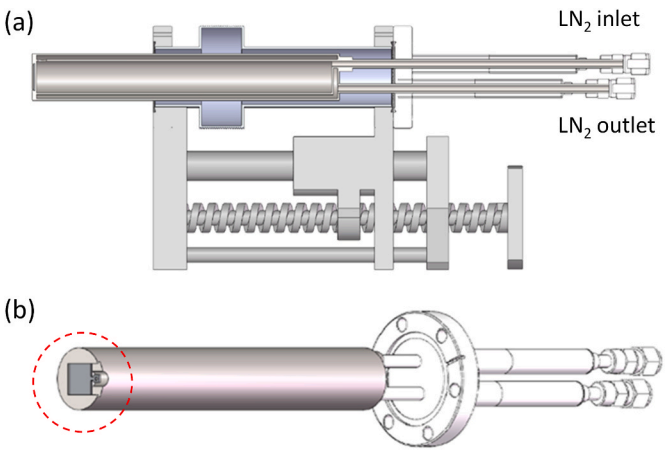

Fig. 2. Schematic drawing of the cryogenic sample stage. (a) The side view with the LN_2 inlet and outlet tubes are indicated. (b) The tilted view showing the sample position.

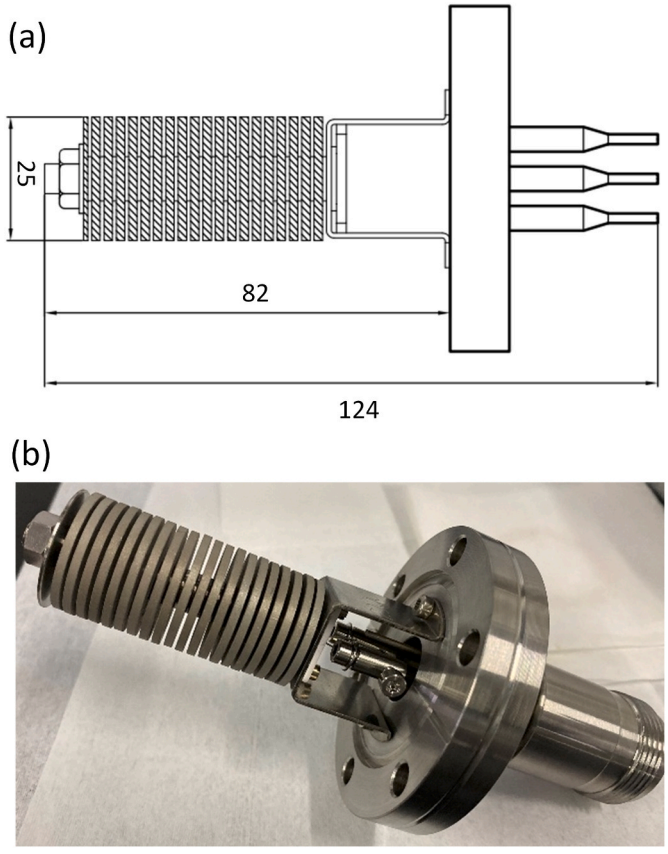

Fig. 3. (a) The structure and dimension of the NEG pump. (Unit: mm) (b) the photo of the NEG pump used in the vacuum suitcase.

Besides the high pumping speed and vacuum limit (<10^{-8} mbar), the NEG pump also has the advantage of power free and light weight [20, 21]. Comparing with the normal vacuum suitcase with battery powered ion getter pump, our system could reduce the weight of the magnet and VRLA battery, which is a few kilograms. More importantly, abandoning the dependence to battery allows the users to choose train or cars for shipping between labs of long distance. The low pumping speed of NEG for noble gas could be solved by thorough baking out to reduce the concentration in the residue gas. Test result shows that with at 140 °C, our system could maintain below 10^{-8} mbar for 5 h and below 10^{-7} mbar for 20 days, which satisfies the requirement of sensitive 2D materials. Detailed of testing on a prototype system is discussed in the following section.

3. Simulation and prototype model testing

3.1. Simulation of the cryogenic sample stage

The sample stage is mounted on a double wall LN_2 container assembled on a linear motion, as show in Fig. 4(a). The inner tank, 125 mL volume inside the inner wall, contains the liquid phase cryogen LN_2, while the outer tank, 37 mL volume between the inner and outer wall, contains the evaporated gas phase cold N_2. In order to verify the performance of cooling, mainly the minimum temperature and holding time, we adopted the finite element simulation with the software COMSOL 5.4. Considering that the cryogen in the container is in static state, we adopted the multi-physical field coupling module of solid heat transfer and surface radiation, taking LN_2 as the cryogen. The whole working process can be divided into 3 stages according to the residual amount of LN_2, as shown in Fig. 4(b). In stage 1, LN_2 continuously flows into the full container while the sample is well-cooled. In stage 2, the LN_2 supply stops and the liquid in the container gradually evaporates until dry up, while the sample maintains the low temperature. In stage 3, the container is empty and the sample warms up naturally. In these processes, there are two key points that we concerned: the first one is the minimum temperature of the sample; the second one is the low temperature holding time in stage 2, which determines the time for optical measurement.

In stage 1, the system reaches thermal equilibrium. The temperature field $\boldsymbol{u}$ of the system can be described by the following solid heat transfer equation:

$$\frac{\partial \boldsymbol{u}}{\partial t} = \frac{K}{\rho C}\left(\frac{d^2\boldsymbol{u}}{dx^2} + \frac{d^2\boldsymbol{u}}{dy^2} + \frac{d^2\boldsymbol{u}}{dz^2}\right) = 0$$

Where K is the thermal conductivity, ρ is the material density, and C is the specific heat of the material. SS316 is mainly used in the system, and the values of the three parameters are as follows : K_{SS316} = 16.3 W/(m•K) , ρ_{SS316} = 7.93 g/cm^3 , C_{SS316} = 0.5 kJ/(kg•K). Meanwhile, we also consider the radiative heat transfer inside the system, which can be described as:

$$\boldsymbol{q} = \varepsilon \bullet \mathrm{A}\cdot\sigma\left(T_f^{\,4} - T_w^{\,4}\right)$$

Where ε is the surface refractive index, which is 0.35 for SS316. A is the object surface area. σ is the Stefan constant, $5.67 \times 10^{-8} W \bullet m^{-2} \bullet K^{-4}$. The boundary conditions are set as follows: the interior of container is set as 77 K, and the outer surface of the system is set as natural convection in ambient condition.

In order to reduce unnecessary calculation, we replaced the part of the chamber with blind flange except cryostat. The simulated temperature field distribution of the whole system is shown in Fig. 4(c). Thanks to the efficient heat preservation in the vacuum chamber, the sample stage can be cooled to about 80 K. As shown in the simulation slice temperature field map in Fig. 4(c), the sample temperature can also be

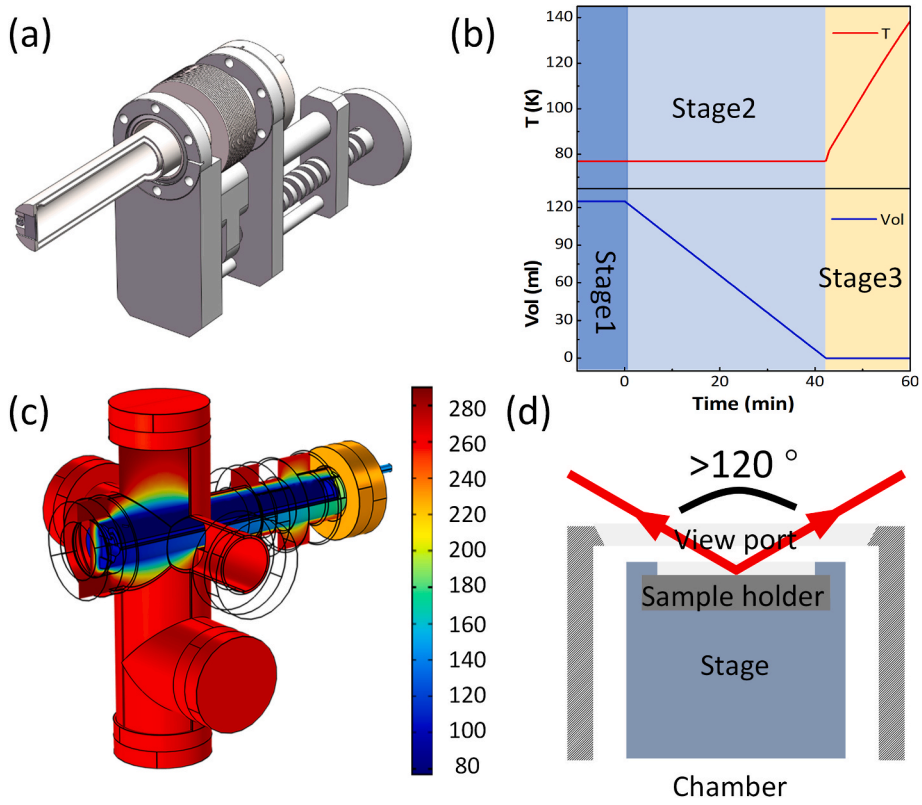

Fig. 4. (a) Partial cross-sectional view of double wall LN_2 container with cryogenic sample stage. (b) The simulated sample temperature and the residual volume of LN_2 in the container as a function of time. (c) The simulated static temperature field of the system when the container was fully filled with LN_2. (d) The schematic diagram of the maximum visual angle during characterization of the sample on cryogenic stage.

maintained at ~ 80 K.

As for the minimum temperature holding time in stage 2, it was estimated according to total radiating power, written as:

$$\Delta T = \frac{\Delta H_1 \bullet m_1 + \Delta H_2 \bullet m_2}{p}$$

ΔH_1 represents the latent heat of phase change of LN_2, and m_1 represents mass of LN2 in the inner tank. ΔH_2 represents the heat tolerance difference between LN2 at 77 K and N2 at average temperature in the outlet, and m_2 represents the mass of N2 in the outer tank. For the total radiating power p, we use the value 8.59 W which is integration over the whole outer surface of the container and stage with sample. The cooling is maintaining mainly by the vaporization by LN2. According to the simulation results in stage 1, the average temperature of the cold gas in the outer tank is 103 K. Therefore, we estimate that the low temperature holding time is 42.3 min, which is basically enough for static optical characterization. If it allows the vibration due to continuous LN2 flow or pumping of cold N2, there will be no constrain of low temperature holding time. Owning to the tunable distance between the sample surface and the glass window, a visual angle as larger as 120° is allowed for the optical characterization of the cooled sample, as demonstrated in Fig. 4(d).

3.2. Testing of the prototype system

To verify the vacuum and sample transfer performance of the design, we have built a prototype system with NEG pump, as shown in Fig. 5(a). Three complete cycles of baking out and vacuum holding tests has been done. The system was connected to a pumping station equipped of a Pfeiffer turbo pump (HiPace 300) and Agilent rotary pump. The vacuum was monitored by BA gauge installed in the main chamber. After 140 °C baking out for 48 h, followed by NEG activation at 30 W for 60 min, the vacuum reached the limit of about 2×10^{-9} mbar. The pressure recorded in Fig. 5(b) started when the mini gate valve to pumping station is closed, which means the vacuum is maintained only by the NEG pump from that moment on.

The pressure curve shows two stages in the vacuum holding period. In the first stage, the pressure gradually increased until a stable value of 2×10^{-8} mbar in 2.5 days. In the beginning of this stage, it was maintained below 1×10^{-8} mbar for 5 h, as shown in Fig. 5(c). In the second stage, the vacuum is remains stable around 2–3 $\times 10^{-8}$ mbar range with some fluctuation. The broad peak at day 12–13 is due to a temporary room temperature fluctuation in the lab caused by baking out of another system. The vacuum test was terminated at Day 20 when the pressure was about 4×10^{-8} mbar. We anticipate the vacuum will stay below 5×10^{-8} mbar for a few more days, which is already beyond the requirement.

To test the leakage rate of the system, a prolonged pressure measurement was performed after the saturation of the NEG pump, as shown in Fig. 5(d). The linear part in the pressure-time curve is due to the leakage. The leakage rate is calculated according to the following equation: $Q = V \bullet \frac{\Delta P}{\Delta t} = V(P_2 - P_1)/(t_2 - t_1)$. The volume of the system V = 2.6 L; the ΔP and Δt are indicated by the double arrows in Fig. 5(d). It is measured that $\Delta P = 1.94 \times 10^{-4}$ mbar and $\Delta t = 9.4 \times 10^5$ s. Therefore, the leakage rate can be calculated as $Q = 5.4 \times 10^{-10}$ mbar • L/s, which fulfilled the requirement of our design.

A test measurement on an isolated prototype cryogenic stage shows that a minimum temperature of ~84 K can be realized in 90 min, as demonstrated in Fig. 5(e). Although further optimized is still needed, the result generally proved that our design is practical.

3.3. Sample exchange and STM characterization

To test the sample exchange and vacuum performance for real 2D material, we have transferred as grown multi-domain monolayer $MoTe_2$ film from the MBE system to a LT-STM system at another location of our campus. The film is sensitive to air due to the dangling bonds at the domain boundaries and surface of ferroelectric 1T' phase. Therefore, this sample is suitable to evaluate the vacuum performance. Fig. 6(a) shows photo of the prototype vacuum suitcase connected to a LT-STM system (Createc). The height adapted by using an extra frame with adjustable legs. Such a stable connection and the fine-tuning mechanism of the transfer rod facilitate a very smooth and quick sample exchange, as shown in Fig. 6(b).

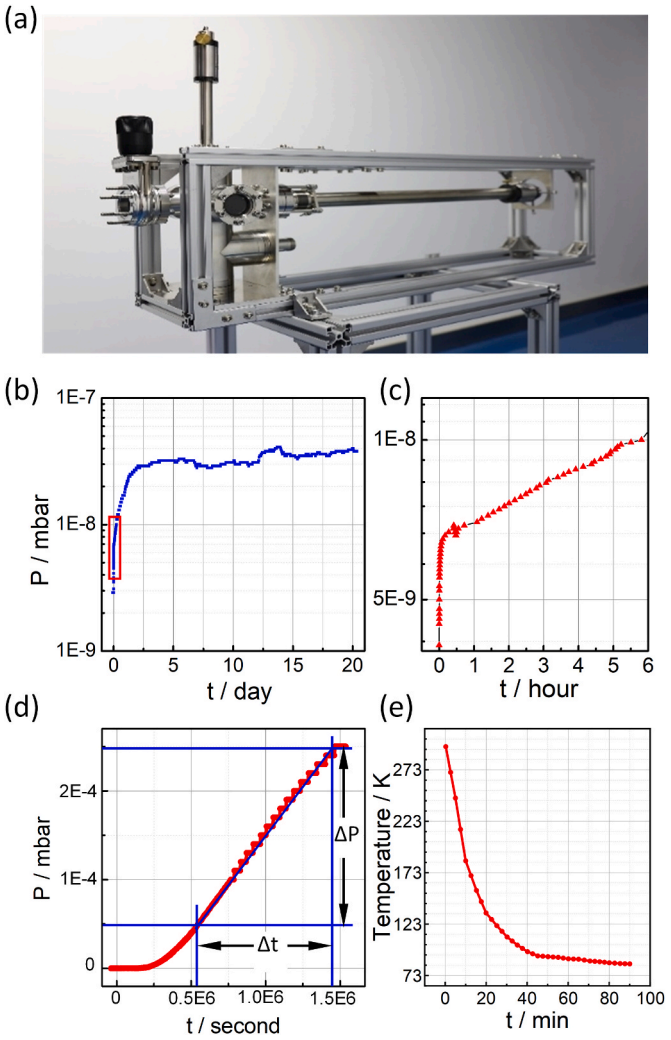

Fig. 5. (a) The photograph of the prototype system used for testing. (b) The measured pressure vs time for 22 days. (c) Enlarged region in (b) as indicated by the red rectangle, displaying the pressure in the first 6 h. (d) The pressure vs time curves measured for leakage test. The linear regions are indicated for calculating the leakage rate. (e) The cooling curve measured on a testing cryogenic stage.

The sample was stored in the suitcase for about 10 h prior to loading into the STM. The time was spent on pumping down (~2 h) and briefly bakeout (~8 h) of the small space between the suitcase and the STM main chamber. The transferred sample was directly loaded into the LT-STM for characterization at 78 K. As shown in the overview topographic STM image in Fig. 6(c), the monolayer $MoTe_2$ film displays terraces with sharp step edges. The zoom-in image in Fig. 6(d) shows the neighboring 2H-$MoTe_2$ and 1T′-$MoTe_2$ domains with a clean domain boundary. The bright feature decorating the step edges are actually Mo_6Te_6 nanowires as reported in another work of us [22]. The sample surface is free of physically adsorbed molecular contaminates, as proved by the atomic resolution image of 1T′-$MoTe_2$ in Fig. 6(e). The irregular metallic edges

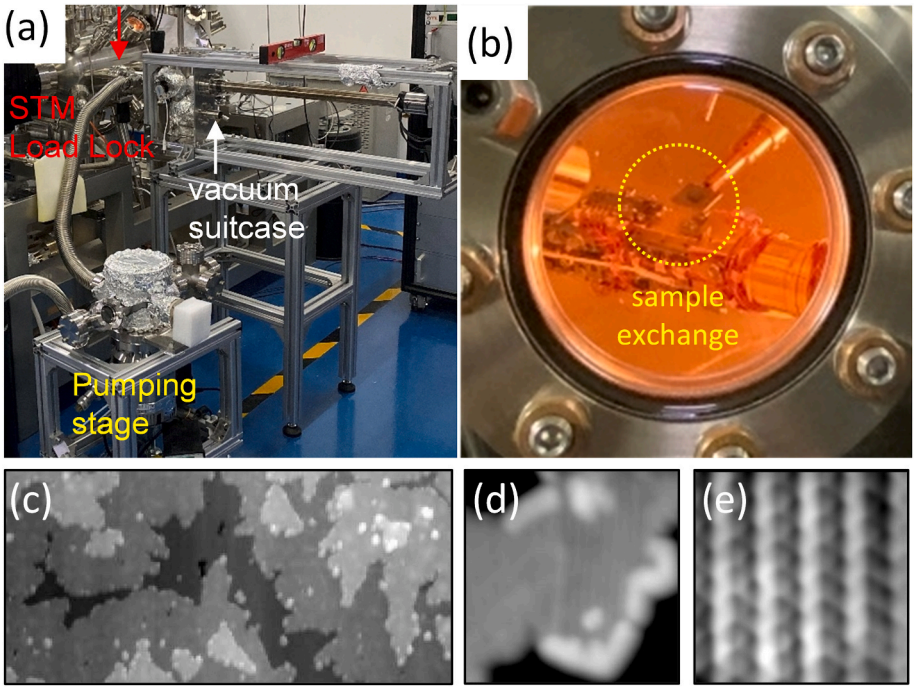

Fig. 6. (a) Photograph showing the prototype vacuum suitcase connected to a UHV STM system. (b) Photograph showing transfer of a flag type sample holder. (c) Overview STM image of $MoTe_2$ film on HOPG. Image parameters:75 × 150 nm^2, 2 V, 20 pA. (d) The zoom-in image of neighboring 2H-$MoTe_2$ and 1T′-$MoTe_2$ domains. Image parameters: 16.6 × 16.6 nm^2, 2 V, 20 pA. (e) Atomic resolution of 1T′-$MoTe_2$ domain with clean surface. Image parameters: 3.2 × 3.2 nm^2, 3 mV, 2 nA.

of the TMDC islands due to oxidation during air exposure, as reported in the literature [23], has been nicely avoided by using vacuum transfer. Therefore, the testing results proved that the performance of the vacuum suitcase could fulfill our requirement.

4. Summary

In summary, we have designed a compact power free multifunctional vacuum suitcase specially for the transfer and investigation of the MBE grown sensitive 2D materials that would be quickly contaminated if exposed to ambient condition. The vacuum suitcase could store and transfer up to 5 samples supported by the commonly used flag type sample holders. It could also be used for the low temperature optical characterizations (Raman spectroscopy etc.) by incorporating a LN_2 cooled cryogenic sample stage in the system. Based on finite element simulation results, it was confirmed that the minimum sample temperature could reach ~80 K and hold that temperature for 42 min within one refilling cycle of the LN_2 container. The test on home-built prototype system shows it could maintain the vacuum at 10^{-8} mbar level for 5 h and 10^{-7} mbar level for more 20 days. Sample transfer and *ex situ* characterization was also successfully tested on an UHV STM. We anticipate such highly custom designed and specialized research equipment would greatly facilitate the characterization sensitive 2D materials and devices.

CRediT authorship contribution statement

Dongli Wang: Writing – review & editing, Writing – original draft, Visualization, Validation, Investigation, Formal analysis, Data curation. **Di Wu:** Writing – original draft, Visualization, Validation, Software, Methodology, Investigation, Data curation. **Songjie Feng:** Visualization, Software, Methodology. **Yuang Li:** Writing – review & editing, Data curation. **Tai Min:** Validation, Supervision. **Yi Pan:** Writing – review & editing, Supervision, Funding acquisition, Conceptualization.

Declaration of competing interest

The authors declare that they have no known competing financial interests or personal relationships that could have appeared to influence the work reported in this paper.

Data availability

Data will be made available on request.

Acknowledgments

Dongli Wang and Di Wu contributed equally to this work. We acknowledge support from the National Natural Science Foundation of China (Grant No. 12074302), the Strategic Priority Research Program of the Chinese Academy of Sciences (Grant No. XDB30000000), the National Key R&D Program of China (Grant No. 2022YFA1200087), and the Fundamental Research Fundings for the Central Universities.

References

[1] P. Li, C. Wang, J. Zhang, S. Chen, D. Guo, W. Ji, D. Zhong, Single-layer CrI3 grown by molecular beam epitaxy, Sci. Bull. 65 (2020) 1064–1071, https://doi.org/10.1016/j.scib.2020.03.031.
[2] W. Chen, Z. Sun, Z. Wang, L. Gu, X. Xu, S. Wu, C. Gao, Direct observation of van der Waals stacking–dependent interlayer magnetism, Science 366 (2019) 983, https://doi.org/10.1126/science.aav1937.
[3] S. Liu, X. Yuan, Y. Zou, Y. Sheng, C. Huang, E. Zhang, J. Ling, Y. Liu, W. Wang, C. Zhang, et al., Wafer-scale two-dimensional ferromagnetic Fe3GeTe2 thin films grown by molecular beam epitaxy, npj 2D Mater. Appl. 1 (2017), https://doi.org/10.1038/s41699-017-0033-3.
[4] M. Mogi, A. Tsukazaki, Y. Kaneko, R. Yoshimi, K.S. Takahashi, M. Kawasaki, Y. Tokura, Ferromagnetic insulator Cr2Ge2Te6 thin films with perpendicular remanence, Apl. Mater. 6 (2018), 091104, https://doi.org/10.1063/1.5046166.
[5] W. Ding, J. Zhu, Z. Wang, Y. Gao, D. Xiao, Y. Gu, Z. Zhang, W. Zhu, Prediction of intrinsic two-dimensional ferroelectrics in In2Se3 and other III2-VI3 van der Waals materials, Nat. Commun. 8 (2017), 14956, https://doi.org/10.1038/ncomms14956.
[6] S. Yuan, X. Luo, H.L. Chan, C. Xiao, Y. Dai, M. Xie, J. Hao, Room-temperature ferroelectricity in MoTe2 down to the atomic monolayer limit, Nat. Commun. 10 (2019) 1775, https://doi.org/10.1038/s41467-019-09669-x.
[7] J. Hall, N. Ehlen, J. Berges, E. van Loon, C. van Efferen, C. Murray, M. Rosner, J. Li, B.V. Senkovskiy, M. Hell, et al., Environmental control of charge density wave order in monolayer 2H-TaS2, ACS Nano 13 (2019) 10210–10220, https://doi.org/10.1021/acsnano.9b03419.
[8] P. Tsipas, D. Tsoutsou, S. Fragkos, R. Sant, C. Alvarez, H. Okuno, G. Renaud, R. Alcotte, T. Baron, A. Dimoulas, Massless Dirac fermions in ZrTe2 semimetal grown on InAs(111) by van der Waals epitaxy, ACS Nano 12 (2018) 1696–1703, https://doi.org/10.1021/acsnano.7b08350.

[9] K. Sugawara, Y. Nakata, R. Shimizu, P. Han, T. Hitosugi, T. Sato, T. Takahashi, Unconventional charge-density-wave transition in monolayer 1T-TiSe2, ACS Nano 10 (2016) 1341–1345, https://doi.org/10.1021/acsnano.5b06727.
[10] S. Tang, C. Zhang, D. Wong, Z. Pedramrazi, H.-Z. Tsai, C. Jia, B. Moritz, M. Claassen, H. Ryu, S. Kahn, et al., Quantum spin Hall state in monolayer 1T'-WTe2, Nat. Phys. 13 (2017) 683–687, https://doi.org/10.1038/nphys4174.
[11] S. Tang, C. Zhang, C. Jia, H. Ryu, C. Hwang, M. Hashimoto, D. Lu, Z. Liu, T. P. Devereaux, Z.-X. Shen, et al., Electronic structure of monolayer 1T′-MoTe2 grown by molecular beam epitaxy, Apl. Mater. 6 (2017), 026601, https://doi.org/10.1063/1.5004700.
[12] D. Shcherbakov, P. Stepanov, D. Weber, Y. Wang, J. Hu, Y. Zhu, K. Watanabe, T. Taniguchi, Z. Mao, W. Windl, et al., Raman spectroscopy, photocatalytic degradation, and stabilization of atomically thin chromium tri-iodide, Nano Lett. 18 (2018) 4214–4219, https://doi.org/10.1021/acs.nanolett.8b01131.
[13] B.F. Hu, P. Zheng, R.H. Yuan, T. Dong, B. Cheng, Z.G. Chen, N.L. Wang, Optical spectroscopy study on CeTe3: evidence for multiple charge-density-wave orders, Phys. Rev. B 83 (2011), https://doi.org/10.1103/PhysRevB.83.155113.
[14] L. Yuan, B. Zheng, J. Kunstmann, T. Brumme, A.B. Kuc, C. Ma, S. Deng, D. Blach, A. Pan, L. Huang, Twist-angle-dependent interlayer exciton diffusion in WS2–WSe2 heterobilayers, Nat. Mater. 19 (2020) 617–623, https://doi.org/10.1038/s41563-020-0670-3.
[15] P. Jiříček, M. Cukr, V. Kolařık, S. Koc, Transfer of samples between separated ultrahigh vacuum instruments for semiconductor surface studies, Rev. Sci. Instrum. 69 (1998) 2804–2805, https://doi.org/10.1063/1.1148982.
[16] C.D. Park, S.M. Chung, P. Manini, Combination of compact nonevaporable getter and small ion pumps for ultrahigh vacuum systems, J. Vac. Sci. Technol. 29 (2011), 011012, https://doi.org/10.1116/1.3529379.
[17] Y. Watanabe, Y.F. Nishimura, R. Suzuki, H. Uehara, T. Nimura, A. Beniya, N. Isomura, K. Asakura, S. Takakusagi, Portable ultrahigh-vacuum sample storage system for polarization-dependent total-reflection fluorescence x-ray absorption fine structure spectroscopy, J. Vac. Sci. Technol. 34 (2015), 023201, https://doi.org/10.1116/1.4936344.
[18] K. Hou, J. Li, T. Qu, B. Tang, L. Zhu, Y. Huang, H. Li, Development of a suitcase time-of-flight mass spectrometer for in situ fault diagnosis of SF6-insulated switchgear by detection of decomposition products, Rapid Commun. Mass Spectrom. 30 (2016) 38–43, https://doi.org/10.1002/rcm.7624.
[19] A.S. Mohd, S. Puetter, S. Mattauch, A. Koutsioubas, H. Schneider, A. Weber, T. Brueckel, A versatile UHV transport and measurement chamber for neutron reflectometry under UHV conditions, Rev. Sci. Instrum. 87 (2016), https://doi.org/10.1063/1.4972993.
[20] H. Kodama, S. Ohno, M. Tanaka, M. Tanaka, K.K. Okudaira, K. Mase, T. Kikuchi, Low-cost, high-performance nonevaporable getter pumps using nonevaporable getter pills, J. Vac. Sci. Technol. 34 (2016), 051601, https://doi.org/10.1116/1.4961050.
[21] M.L. Stutzman, P.A. Adderley, M.A.A. Mamun, M. Poelker, Nonevaporable getter coating chambers for extreme high vacuum, J. Vac. Sci. Technol. 36 (2018), 031603, https://doi.org/10.1116/1.5010154.
[22] Y.A. Li, D. Wu, D.L. Wang, Y.N. Zhang, T. Min, Y. Pan, Atomic-scale observation of the local structure and 1D quantum effects in vdW stacking Mo6Te6 nanowires, Adv. Mater. Interfac. (2022) 2202043, https://doi.org/10.1002/admi.202202043.
[23] R. Addou, C.M. Smyth, J.Y. Noh, Y.C. Lin, Y. Pan, S.M. Eichfeld, S. Fölsch, J. A. Robinson, K. Cho, R.M. Feenstra, R.M. Wallace, One dimensional metallic edges in atomically thin WSe2 induced by air exposure, 2D Mater. 5 (2018), 025017, https://doi.org/10.1088/2053-1583/aab0cd.